

GEANT3 Simulation of Detector Shielding Wall Design

K. E. Myers

The George Washington University
Washington, D.C.

Abstract

The task of simulating a design for the upstream wall of the detector shielding hut was started in the middle of January 2008. We were given until the end of March 2008 to finish the design and came close to meeting this goal, handing the final design to Paulo Medeiros on April 21, 2008. The task was to optimize the aperture and material of the wall in the space allowed, 80 cm from $Z = 300$ to $Z = 380$ cm. This note describes the different designs tested and presents backgrounds for the varying cases. It is important to note that these simulations do not consider every type or every source of backgrounds. The background most sensitive to the addition of a shielding wall is from inelastics so the goal was to minimally interact with these while reducing the solid angle of backgrounds seen by the detector. In the end an 80 cm concrete wall was chosen which yields inelastic backgrounds on the order of about 0.6%¹.

¹The value quoted uses a new inelastic generator. For most of this note the results presented are from using an old inelastic generator that produces backgrounds 5 times too large. Correct values for the new inelastic generator are presented in Section 5

Contents

1	Introduction	5
2	Defining the envelope	5
3	Concrete wall	7
3.1	Flaring the sides	8
3.2	Changing the upper aperture	9
4	Concrete and lead wall	11
4.1	Changing the thickness	13
4.2	Changing the upper clearance	14
5	New inelastic generator	14
5.1	Problems with the old generator	15
5.2	Results	16
6	Concrete and lead wall - realistic	16
6.1	Concrete wall thickness	16
7	Summary of results	19
8	Conclusions	19

List of Figures

1	Side view and top view of the elastic electron envelope for BFIL 1.02, 1.04, and 1.06 in the shielding wall space.	6
2	Worst case scenario of misalignment of the Čerenkov bars. From [1].	6
3	XZ origin (side view) and YZ origin (top view) plots of the inelastic electron origin in an 80 cm concrete wall.	8
4	Comparing the Y origin of inelastic electrons in the wall for straight sides (black) and flared sides (blue).	9
5	X profile of elastic (blue) and inelastic (red) electrons at $Z = 300$ cm.	10
6	Comparing the Z origin of inelastic electrons in the wall with the aperture parallel to the elastics (black) and parallel to the inelastics (blue).	11
7	Z origin of inelastic electrons (left) and inelastic photons (right) in the shielding wall for an 80 cm wall with no lead backing (black), 5.08 cm lead backing (red) and 10.16 cm lead backing (blue).	12
8	Locations of the elastic upper edge (blue), the inelastic peak (red), and the wall aperture (black), from $Z = 300$ cm to $Z = 380$ cm.	13
9	Inelastic backgrounds as a function of upper clearance for a 35 cm concrete + 5 cm lead wall at $Z = 300 - 340$ cm.	14
10	Inelastic rate as a function of upper θ with the old inelastic generator. (Figure from Juliette Mammei.)	15
11	XZ origin of inelastic electrons in a 40 cm concrete wall and the 1-D X projection.	17
12	XZ origin of Møller electrons in a 40 cm concrete wall and the 1-D X projection.	18
13	Inelastic and Møller backgrounds as a function of concrete wall thickness.	18
14	Side-angle view of the GEANT3 simulation geometry with the shielding wall.	20

List of Tables

1	Elastic electron envelope cutoffs for BFIL 1.02, 1.04, and 1.06, in the shielding wall space.	6
2	Background comparison of no wall and an 80 cm concrete wall.	7
3	Background comparison of apertures with flared sides.	9
4	Background comparison of an aperture parallel to elastics and parallel to inelastics.	11
5	Background comparison of an 80 cm wall with different amounts of lead backing.	12
6	Background comparison of a 35 cm concrete + 5 cm of lead wall at different Z locations.	13
7	Inelastic backgrounds for the old versus new inelastic generator.	16
8	Background comparison of a 40 cm wall with and without a 5 cm lead backing.	17
9	Summary of inelastic and Møller backgrounds.	19

1 Introduction

The goal of the shielding wall simulations was to design an aperture that reduces the solid angle of backgrounds seen by the Čerenkov detector and minimizes backgrounds. The maximum amount of space available for the shielding wall is 80 cm, leaving less than 50 cm between the wall and the downstream end of QTOR. Events were generated in only one octant covering $\theta = 2.5^\circ$ - 19.5° and $\phi = -17^\circ$ - 17° . A BFIL factor of 1.04 was used with the Čerenkov bar located at $Z = 570$ cm and a radial coverage of $X = 319 - 337$ cm. The geometry file contained the collimators, collimator shielding hut, QTOR coils, lintels, floor, and basic beamline. Shielding concrete is assumed with a density of 2.7 g/cm^3 . Reported backgrounds are all weighted properly by cross section, photoelectric efficiency, and asymmetry.

2 Defining the envelope

The first step was to precisely define the primary electron beam envelope through the space of $Z = 300$ to $Z = 380$ cm. The method agreed upon was to define the “cut off” as 0.1% of the peak of the accepted envelope. For the purpose of this definition, the accepted envelope is defined by elastically scattered electrons that hit the actual bar plus 2 cm in both directions radially and plus 1 cm in both directions horizontally. This means the bar has an effective area of $22 \text{ cm} \times 202 \text{ cm}$ compared to the actual size of $18 \text{ cm} \times 200 \text{ cm}$. So that a range of beam energies or BFIL factors could be viable options, three cases were explored in determining acceptable tolerances on clearance: BFIL 1.02, BFIL 1.04, and BFIL 1.06. For each case the radial position of the bar was changed so that the profile fit nicely on the bar. That gave a radial position for the bar of $X = 314 - 336$ cm, $X = 317 - 339$ cm, and $X = 319 - 341$ cm for BFIL 1.02, 1.04, and 1.06, respectively. Figure 1 shows the resulting cutoffs of the elastic electron profile in the wall in a side view and top view.

As seen in Table 1, the cutoff on the sides of the envelope is independent of BFIL. It is important to point this out because in these cases the bar is defining the profile. Above BFIL 1.04 the profile starts to “spill” off the bar horizontally due to defocusing in ϕ by the magnetic field. These electrons are high energy, on the order of 1 GeV. However, any systematic effect of this loss of events is accounted for in Jim Burchall’s systematic studies.

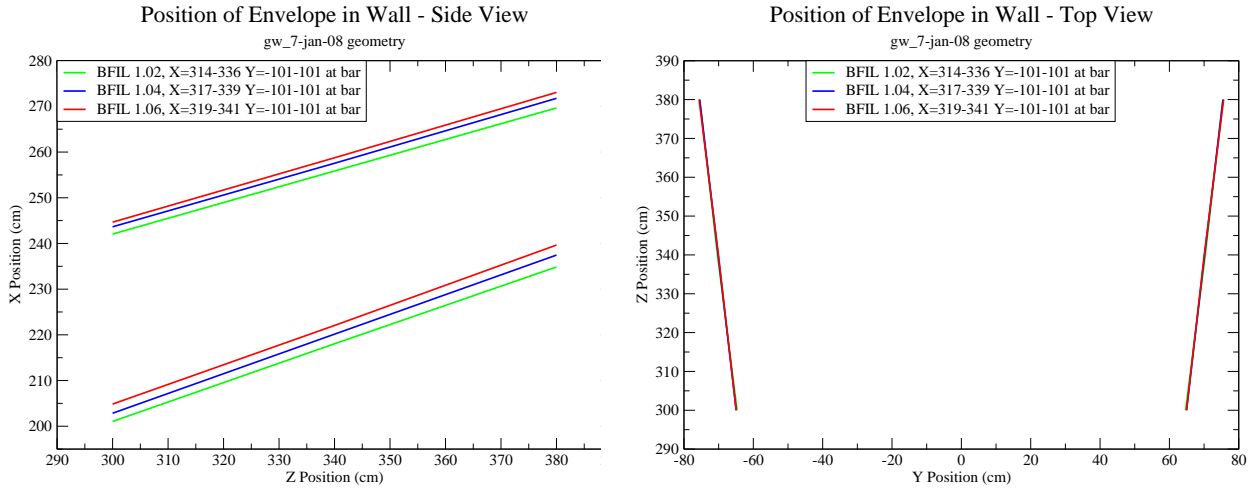


Figure 1: Side view and top view of the elastic electron envelope for BFIL 1.02, 1.04, and 1.06 in the shielding wall space.

	Z = 300	Z = 380
BFIL	Lower Edge Upper Edge Side Edge	Lower Edge Upper Edge Side Edge
1.02	201.05 242.05 ± 64.65	234.85 269.65 ± 75.45
1.04	202.85 243.65 ± 64.95	237.45 271.75 ± 75.45
1.06	204.85 244.65 ± 64.95	239.65 273.05 ± 75.65

Table 1: Elastic electron envelope cutoffs for BFIL 1.02, 1.04, and 1.06, in the shielding wall space.

From a worst case misalignment scenario, illustrated by Fig. 2, a 1.9 cm radial displacement results in a false asymmetry of 6×10^{-10} [1].

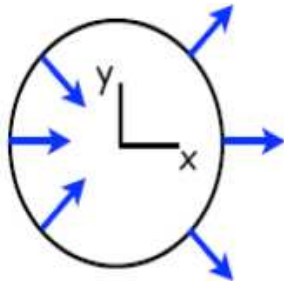


Figure 2: Worst case scenario of misalignment of the Čerenkov bars. From [1].

Based on these findings, it was decided that the side clearance could be no less than 3 cm due to assumed construction and alignment tolerances. The clearance on the lower edge could be no less than 5 cm due to tolerances and the variation of the elastic envelope lower edge with BFIL. With these limits on the sides and lower part of the aperture, the separation between the lower edges of two adjacent windows (or alternatively, the thickness of the spokes at the lower edge of the windows) is only about 26 cm. The wall will be reinforced with stainless steel rebar for support based on Paulo’s recommendation.

3 Concrete wall

The first design for a shielding wall used an upper edge clearance of 20 cm with side and lower clearances of 3 cm and 5 cm, respectively. The wall was 80 cm of concrete and the comparison of backgrounds for this wall with the unrealistic no wall scenario is seen in Table 2.

Geometry	Elastic γ (%)	Inelastic γ (%)	Inelastic e^- (%)	Møller γ (%)	Møller e^- (%)
no wall	0.147 ± 0.005	0.067 ± 0.003	0.467 ± 0.018	0.186 ± 0.012	0.714 ± 0.044
80 cm conc.	0.159 ± 0.005	0.467 ± 0.008	3.883 ± 0.063	0.190 ± 0.012	0.264 ± 0.033

Table 2: Background comparison of no wall and an 80 cm concrete wall.

These results demonstrate the sensitivity of the inelastic backgrounds to material being near the scattered envelope. The Møller electron backgrounds, being mostly low energy, are reduced by about 60%. The inelastic electron backgrounds are larger after the wall is added, and the XZ and YZ origin plots of the inelastic electrons in the shielding wall are shown in Fig. 3. The three prominent sources of inelastic electrons in the wall are from slit-edge scattering along the top surface of the aperture, shower leakage out the back, and scattering on the sides of the aperture.

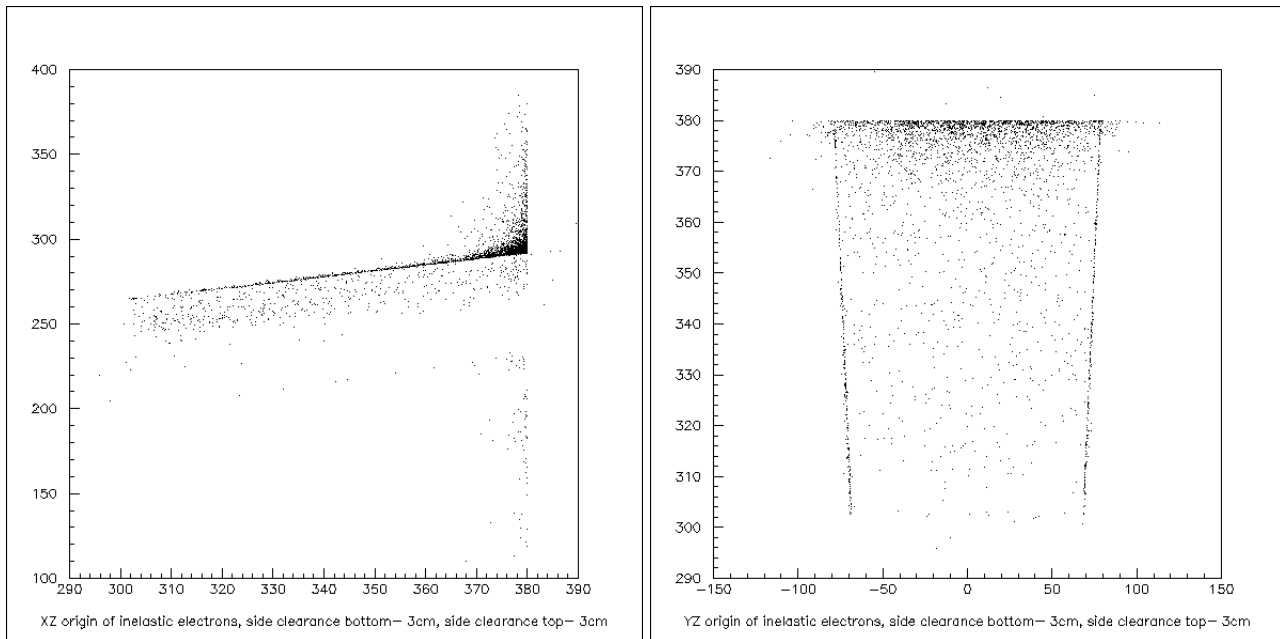


Figure 3: XZ origin (side view) and YZ origin (top view) plots of the inelastic electron origin in an 80 cm concrete wall.

3.1 Flaring the sides

In an attempt to reduce scattering from the sides of the aperture the sides at larger radius were flared, increasing the clearance. The maximum amount of flare, 30 cm, was based on requiring that the thickness of the spokes between octants at the upper corner of the windows be no less than that of the bottom: 26 cm. Other side-upper clearances of 5 cm and 15 cm were also tried. It was determined that 15 cm of clearance on the upper sides was the minimal amount to eliminate scattering from the sides of the aperture. Results for a side-upper clearance of 3 cm, 5 cm, 15 cm, and 30 cm, are compared in Table 3. Møllers are not sensitive to this flaring and so only elastic and inelastic backgrounds are presented.

Flaring the sides so that the side clearance is 3 cm at the lower edge and 15 cm at the upper edge eliminates scattering off the sides of the aperture and reduces the inelastic electron background by 15%.

Side-clearance at large radius (cm)	Elastic γ (%)	Inelastic γ (%)	Inelastic e^- (%)
3	0.159 ± 0.005	0.467 ± 0.008	3.883 ± 0.063
5	0.163 ± 0.005	0.464 ± 0.008	3.800 ± 0.061
15	0.163 ± 0.005	0.409 ± 0.008	3.257 ± 0.056
30	0.166 ± 0.005	0.414 ± 0.008	3.315 ± 0.057

Table 3: Background comparison of apertures with flared sides.

Figure 4 compares the 1-D Y projection of the inelastic electron origin in the wall. The black line is for an aperture with straight sides and the “horns” represent events coming from the sides of the aperture. These horns are eliminated for the flared case, drawn in blue.

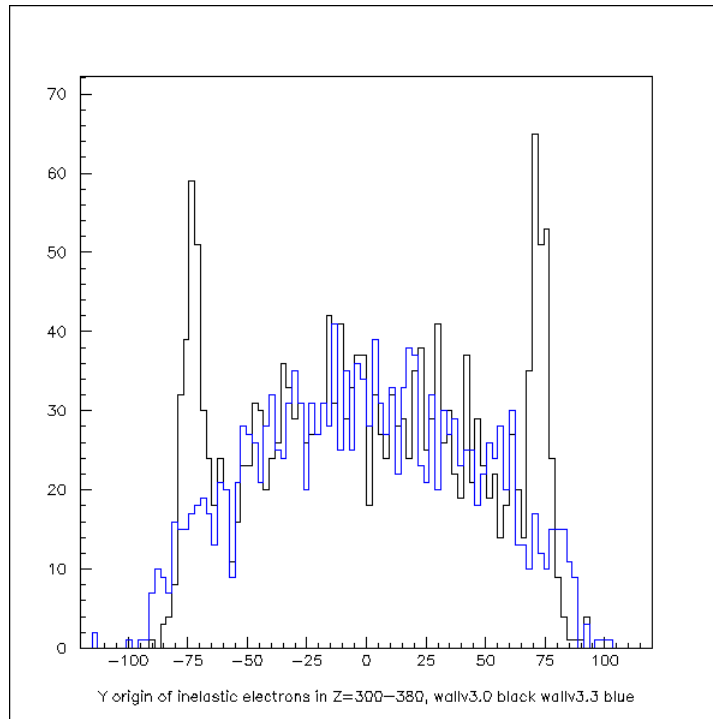


Figure 4: Comparing the Y origin of inelastic electrons in the wall for straight sides (black) and flared sides (blue).

3.2 Changing the upper aperture

In an attempt to reduce inelastic electron showers produced above the aperture in the downstream part of the wall, the upper aperture was changed so that its slope was parallel

to the inelastics. At $Z = 300$ cm, the inelastic peak is at $X = 247.69$ cm and at $Z = 380$ cm it is at $X = 284.66$ cm. At the upstream face of the wall, this gives a separation between the defined upper edge of the elastic electron envelope ($X = 243.65$ cm) and the inelastic peak of only 4.04 cm. The corresponding clearance of the aperture from the inelastic peak is 15.96 cm. Figure 5 shows the elastic electron envelope (blue) with the inelastic electrons (red) at $Z = 300$.

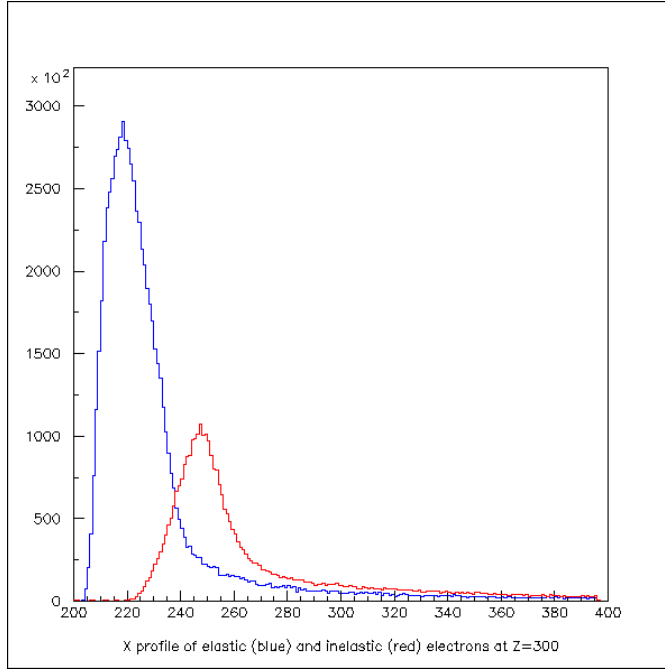


Figure 5: X profile of elastic (blue) and inelastic (red) electrons at $Z = 300$ cm.

At $Z = 380$ cm, the separation between the defined upper edge of the elastic electron envelope ($X = 271.75$ cm) and the inelastic peak is larger, 12.91 cm, giving a clearance of the current aperture from the inelastic peak of only 7.09 cm. At $Z = 300$ cm, the aperture cuts off the inelastics at about 25% of the peak. The corresponding cutoff at $Z = 380$ cm is $X = 302.75$ cm, 11 cm higher than the current aperture. The upper aperture was changed to be parallel to the inelastics with a cutoff of 25% of the inelastic peak. The clearance at the upstream face of the wall remains unchanged, however at the downstream face of the wall the upper aperture is increased by 11 cm. Results comparing backgrounds for an aperture parallel to the elastics versus parallel to the inelastics are shown in Table 4.

Aperture parallel to	Elastic γ (%)	Inelastic γ (%)	Inelastic e^- (%)
elastics	0.163 ± 0.005	0.409 ± 0.008	3.257 ± 0.056
inelastics	0.173 ± 0.005	0.300 ± 0.006	2.704 ± 0.045

Table 4: Background comparison of an aperture parallel to elastics and parallel to inelastics.

There is a reduction in the inelastic electron background of 15%. However, Fig. 6 shows that while there is a decrease in the background coming from shower leakage, there is also an increase in slit-edge scattering. The decision was made to keep the upper aperture parallel to the elastic electron profile, and explore other ways to reduce both slit-edge scattering and shower leakage.

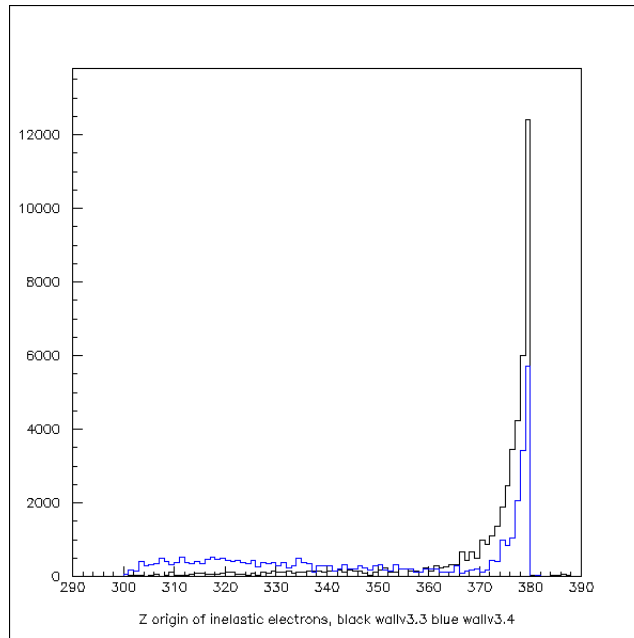


Figure 6: Comparing the Z origin of inelastic electrons in the wall with the aperture parallel to the elastics (black) and parallel to the inelastics (blue).

4 Concrete and lead wall

To reduce showers lead was added to the downstream face of the wall. This study represents unrealistic scenarios in that lead was covering the entire rear face of the wall. Keeping the total thickness of the wall 80 cm, lead backings of 2 inches (5.08 cm) and 4 inches (10.16

cm) were tested. Results for these cases are compared in Table 5.

Amount of lead (cm)	Elastic γ (%)	Inelastic γ (%)	Inelastic e^- (%)
0	0.163 ± 0.005	0.409 ± 0.008	3.257 ± 0.056
5.08	0.159 ± 0.005	0.563 ± 0.009	1.911 ± 0.042
10.16	0.166 ± 0.005	0.470 ± 0.009	1.778 ± 0.040

Table 5: Background comparison of an 80 cm wall with different amounts of lead backing.

Figure 7 shows the Z origin plots of inelastic electrons and inelastic photons for the three cases. The inelastic photon background actually suffers when 2 inches of lead is added to the downstream face of the wall, and then falls to an intermediate value for 4 inches of lead. While the inelastic electron background was reduced by about 40% with the addition of 2 inches of lead, the impact of adding 4 inches of lead on the inelastic electrons is not very significant.

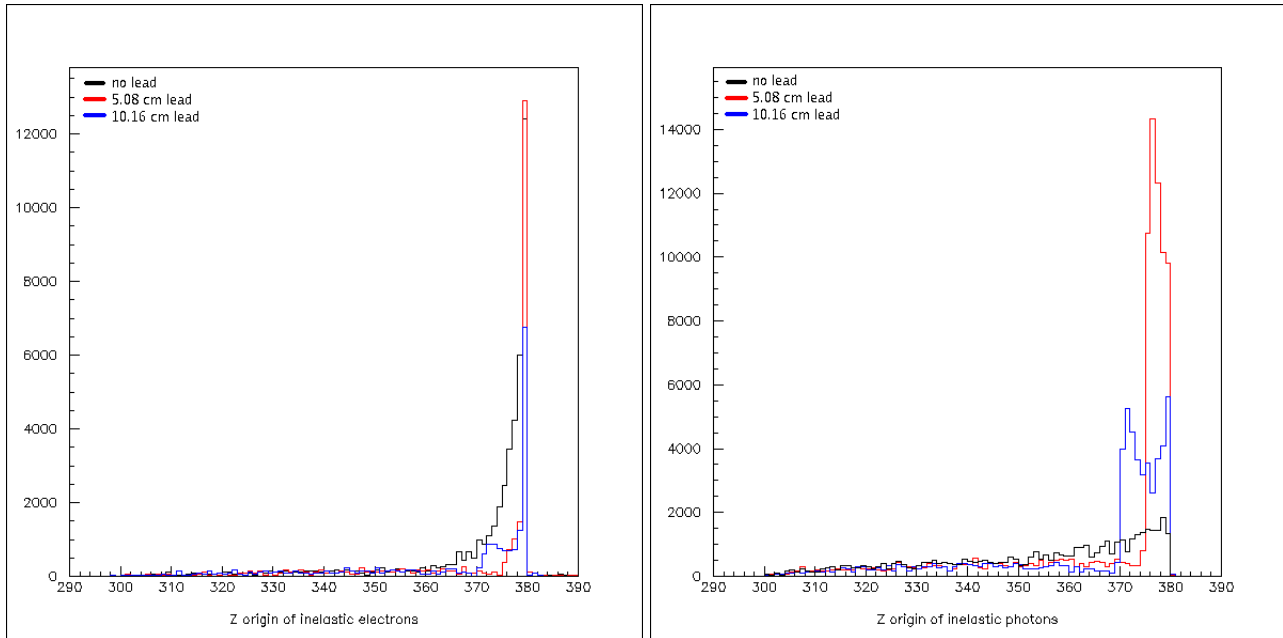


Figure 7: Z origin of inelastic electrons (left) and inelastic photons (right) in the shielding wall for an 80 cm wall with no lead backing (black), 5.08 cm lead backing (red) and 10.16 cm lead backing (blue).

4.1 Changing the thickness

To reduce slit-edge scattering the concrete and lead backed wall was reduced to a total thickness of 40 cm. The cut out of the aperture stayed the same, with the wall being sliced to make it the appropriate thickness. To explore the phase space of Z location, cases of a wall location of $Z = 300 - 340$ cm and $Z = 340 - 380$ cm were compared. These walls are 35 cm of concrete with 5 cm of lead backing, and the inelastic background results are in Table 6.

Z Location (cm)	Inelastic γ (%)	Inelastic e^- (%)
300 - 340	0.389 ± 0.006	1.111 ± 0.027
340 - 380	0.627 ± 0.009	1.718 ± 0.042

Table 6: Background comparison of a 35 cm concrete + 5 cm of lead wall at different Z locations.

The wall located at $Z = 300 - 340$ cm has lower inelastic backgrounds. Figure 8 shows the defined upper edge of the elastic electrons and the inelastic peak from $Z = 300$ cm to $Z = 380$ cm. The separation between the elastic and inelastic electrons is less and the trajectory angles are more similar at the upstream location and thus there is less scraping on the aperture.

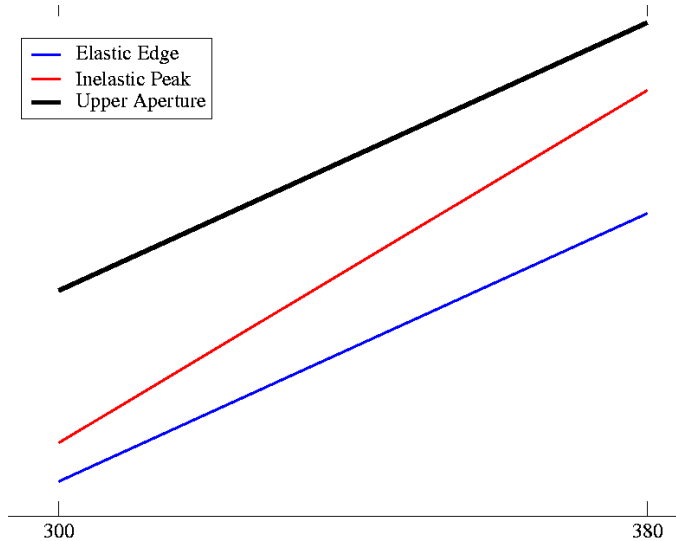


Figure 8: Locations of the elastic upper edge (blue), the inelastic peak (red), and the wall aperture (black), from $Z = 300$ cm to $Z = 380$ cm.

4.2 Changing the upper clearance

With this new wall geometry the upper clearance was varied to see what effect that had on the inelastic backgrounds. The results can be seen in Fig. 9, which shows the inelastic electron and photon backgrounds as a function of upper clearance. The lower-side clearance for all of these cases is fixed at 3 cm, however the upper-side clearance varied. For 20 cm of upper clearance the upper-side clearance is 15 cm, the optimal upper-side clearance that was found in Section 3.1. When the upper clearance was changed, the upper-side clearance changed so that the slope of the sides in the XY plane remained constant.

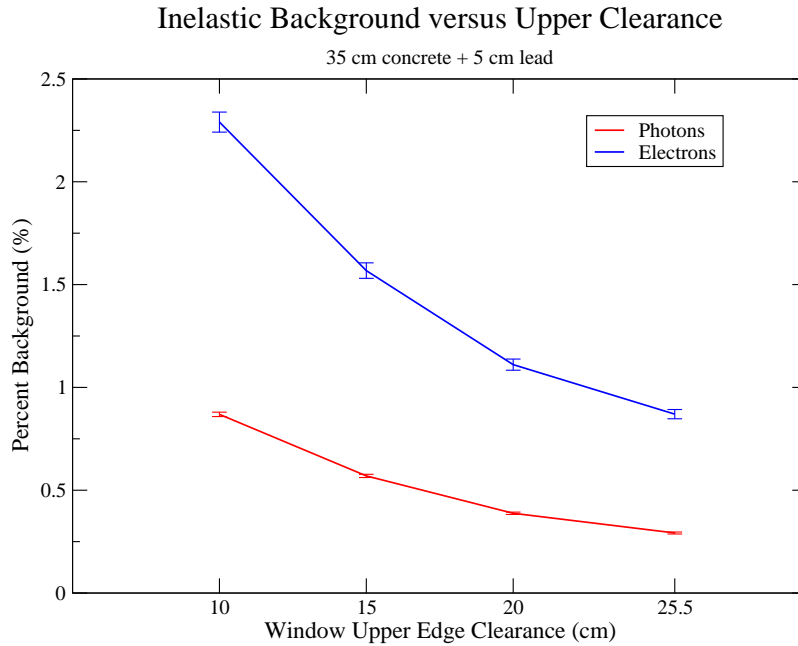


Figure 9: Inelastic backgrounds as a function of upper clearance for a 35 cm concrete + 5 cm lead wall at $Z = 300 - 340$ cm.

5 New inelastic generator

Work with a new inelastic generator was proceeding in parallel to some of these shielding wall geometry tests. Some of the decisions made about a particular geometry (*i.e.* going with an aperture parallel to the elastics, or having an upper clearance of 20 cm versus 25.5 cm) were made based on the results with the new generator. However, simulations with the new inelastic generator were not done for all cases. For the purpose of direct comparison

results so far have been presented with the old inelastic generator values and conclusions based on them are valid for studying relative performance, however not absolute. Although the purpose of this note is not to present work on the inelastic generator problems, a short description is given below.

5.1 Problems with the old generator

In GEANT, the user can specify the θ and ϕ angular range into which events are thrown. When generating primary events in an angular range that is larger than the primary collimator acceptance, further increases in the angular range should not result in a different rate. This holds true for elastic primary events, however when generating inelastic primary events, it was discovered that this was not the case. When the upper limit of the theta range is increased the inelastic rate decreases, as shown in Fig. 10.

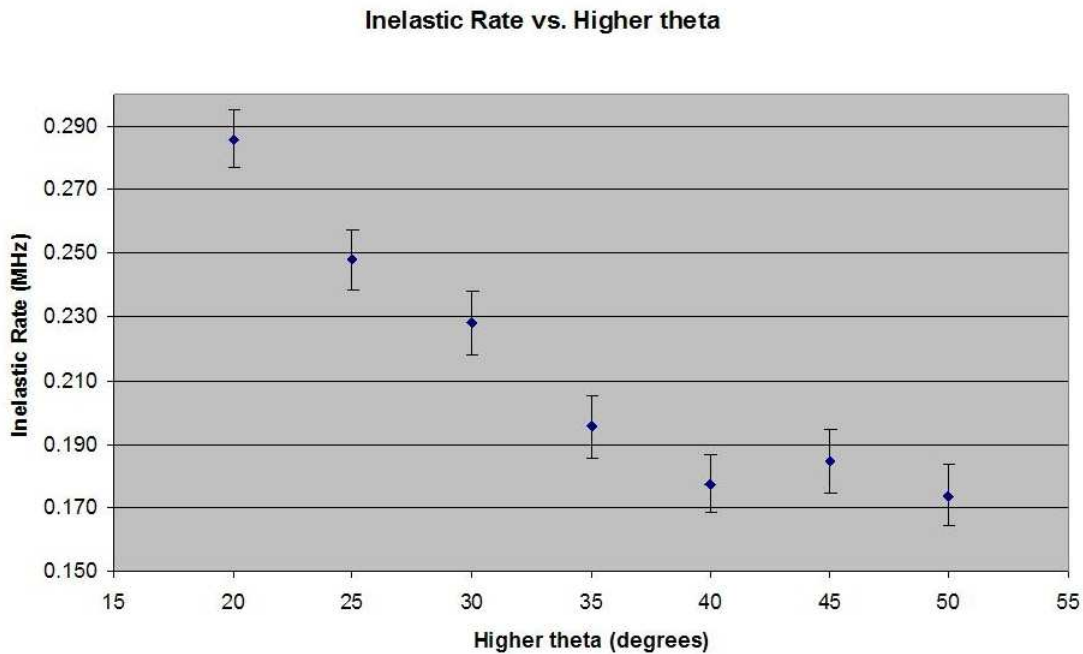


Figure 10: Inelastic rate as a function of upper θ with the old inelastic generator. (Figure from Juliette Mammei.)

Juliette Mammei rewrote the inelastic generator to throw flat in θ , ϕ , and energy and weight the events appropriately².

²For more information, see the Virginia Tech Simulation Group Status Report April 2 2008.

5.2 Results

Inelastic background rates with the new inelastic generator are about 5 times smaller than previous results. Table 7 shows results for some selected geometries comparing backgrounds with the old and new generators. With the new inelastic generator the inelastic backgrounds are reduced and elaborate steps using valuable time, resources, and funds to make further reductions were not needed.

Wall	Inelastic γ (%)-old	Inelastic γ (%)-new	Inelastic e^- (%)-old	Inelastic e^- (%)-new
none	0.067 ± 0.003	0.008 ± 0.001	0.467 ± 0.002	0.095 ± 0.004
80 cm conc.	0.409 ± 0.008	0.076 ± 0.002	3.257 ± 0.006	0.544 ± 0.010
40 cm conc.+lead	0.388 ± 0.006	0.062 ± 0.001	1.111 ± 0.027	0.184 ± 0.005

Table 7: Inelastic backgrounds for the old versus new inelastic generator.

6 Concrete and lead wall - realistic

The next goal was to define a realistic lead backing scenario. The extremes are represented by a 40 cm wall that is all concrete versus a 40 cm wall that has an entire sheet of lead backing.

6.1 Concrete wall thickness

To determine the effect of removing the 5 cm lead backing from the 40 cm thick wall, a baseline scenario of 40 cm of concrete was defined. Table 8 compares the backgrounds for the unrealistic lead case and the bare 40 cm concrete case³. As seen in Table 8, the photon backgrounds are not sensitive to the removal of lead backing. However, the electron backgrounds are very sensitive to this. The inelastic electron background comes primarily from

³Møllers for the unrealistic lead case were not run for this exact aperture. The simulation was run for a 25.5 cm upper clearance, but since the Møllers are not affected by the change in aperture the results for that geometry are a good approximation of the expected results for this geometry. Møller simulations take a few days to run in order to achieve sufficient statistics to be useful.

above the aperture while the Møller electron background comes from below the aperture. Figure's 11 and 12 show the XZ origin of electrons in the 40 cm concrete wall and 1-D X projection for inelastics and Møllers, respectively.

Wall	Inelastic γ (%)	Inelastic e^- (%)	Møller γ (%)	Møller e^- (%)
35 cm conc. + 5 cm lead	0.062 ± 0.001	0.184 ± 0.005	0.268 ± 0.014	0.282 ± 0.033
40 cm conc.	0.061 ± 0.001	0.506 ± 0.008	0.294 ± 0.014	0.609 ± 0.046

Table 8: Background comparison of a 40 cm wall with and without a 5 cm lead backing.

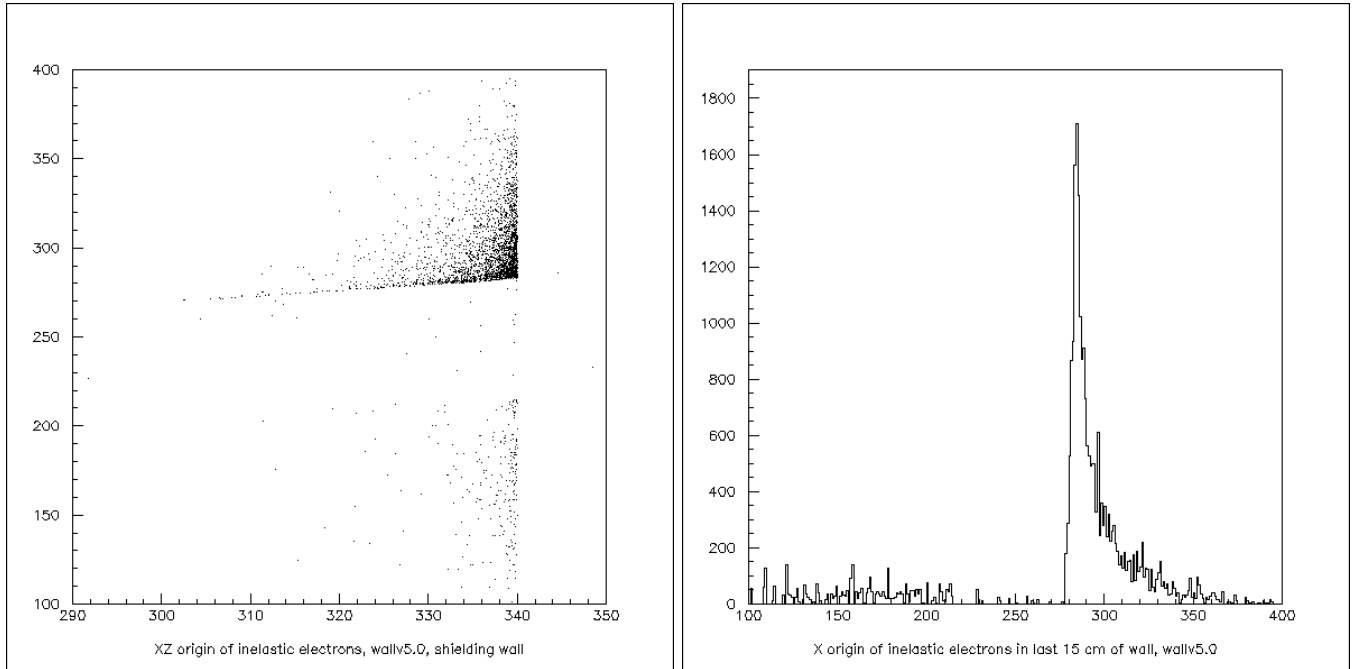


Figure 11: XZ origin of inelastic electrons in a 40 cm concrete wall and the 1-D X projection.

As a basis for comparison, inelastics for a 60 cm concrete wall were simulated. Figure 13 shows the inelastic and Møller backgrounds for concrete walls of thickness 40 cm, 60 cm, and 80 cm. Møller backgrounds for 60 cm were not simulated. The inelastic and Møller electron backgrounds are most affected by the removal of the lead backing.

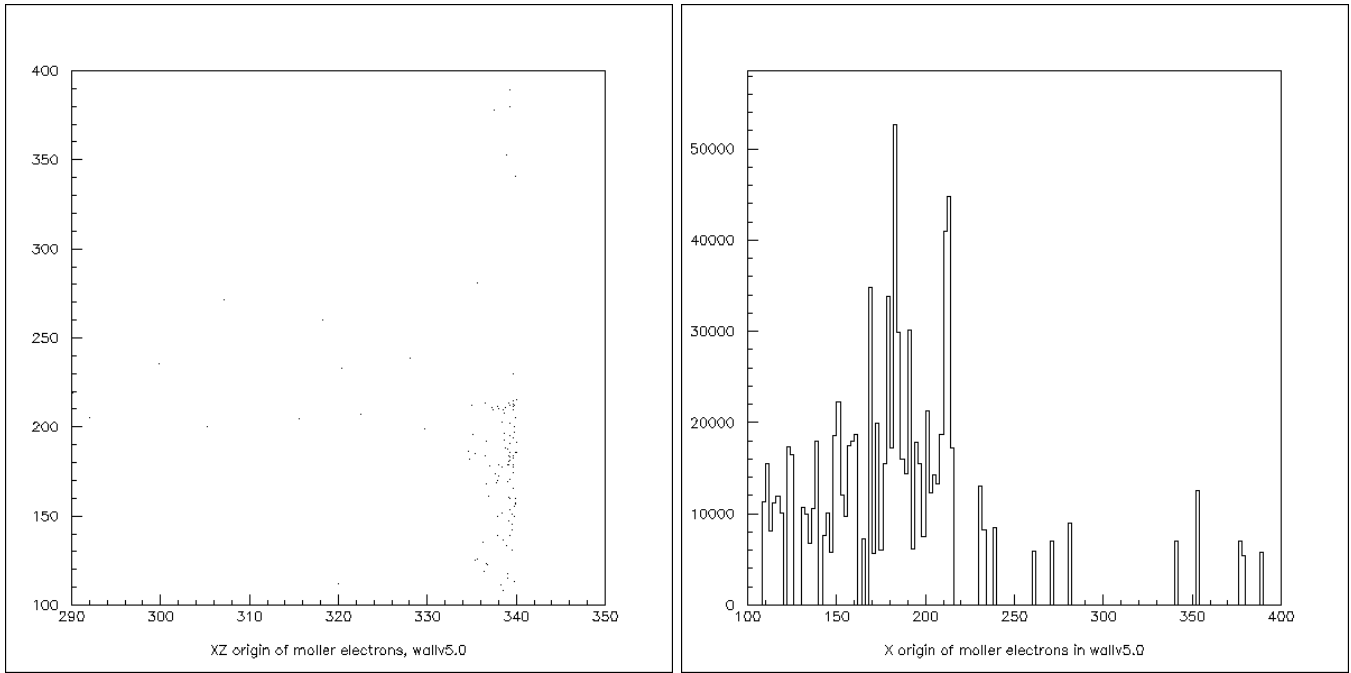


Figure 12: XZ origin of Møller electrons in a 40 cm concrete wall and the 1-D X projection.

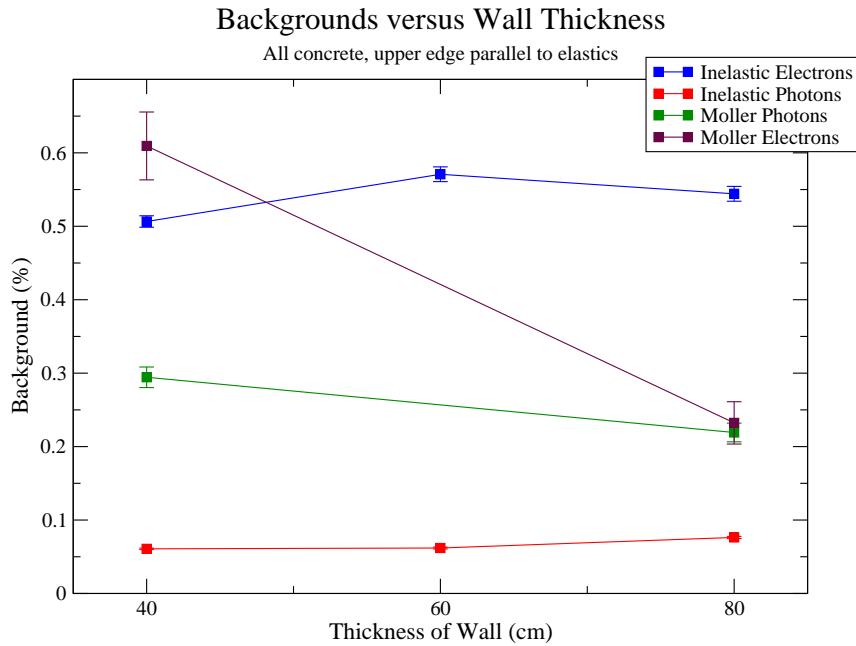


Figure 13: Inelastic and Møller backgrounds as a function of concrete wall thickness.

In order to define a realistic lead scenario there would need to be lead at both the upper and lower edges of the aperture. To cover both areas with sufficient lead to make an impact

would be expensive and not affordable. Assuming a cost of \$2/lb for lead, the lead would cost about \$30,000. This price does not include any costs for mounting and supporting the lead. While in the end no realistic lead geometry was defined, educated estimates can be made about what backgrounds could be achieved.

7 Summary of results

The background budget for Q_{weak} is about 0.7%. With the new inelastic generator the inelastic backgrounds are smaller than previously thought. Table 9 presents a summary of cases studied with inelastic and Møller background values. As mentioned already, a realistic lead case was never defined, but educated estimates can be made. Also, Møller backgrounds for 60 cm of concrete are based on the trend seen in Fig. 13 and Møller backgrounds for the unrealistic lead case are based on a similar geometry as mentioned in footnote 3.

Geometry	Inelastic γ (%)	Inelastic e^- (%)	Møller γ (%)	Møller e^- (%)	Sum(%)
no wall	0.008	0.095	0.186	0.714	1
80 cm conc.	0.076	0.544	0.219	0.232	1.1
60 cm conc.	0.062	0.571	0.257	0.421	1.3
40 cm conc.	0.061	0.506	0.294	0.609	1.5
35 cm conc.+5 cm lead	0.062	0.184	0.268	0.282	0.8
35 cm conc.+5 cm lead real	0.06	?	0.27	?	1

Table 9: Summary of inelastic and Møller backgrounds.

8 Conclusions

The results in Table 9 show that with an 80 cm concrete wall the total background is comparable to the no wall scenario. As mentioned previously in the note, the no wall case looks acceptable, however there are numerous background sources that are not included. The best wall with lead yields backgrounds only 0.3% lower, with the reduction coming from the decrease in inelastic electron background. However, in a realistic lead case only some of this reduction would be achievable due to financial limitations and thus we estimate a realistic

wall with lead may only gain a 0.1% reduction.

Based on these observations, the recommendation was made to design the 80 cm concrete wall. As a reminder, this wall is 80 cm of high-density concrete (2.7 g/cm^3) covering the space $Z = 300 - 380 \text{ cm}$, and has clearances of 5 cm on the bottom, 20 cm on the top, and 3 - 15 cm on the sides (lower-upper side). With more time and more funds it may be possible to design a better wall. However, a simple concrete wall showed results that were ruled to be acceptable and thus was chosen. Figure 14 shows a GEANT3 generated side-angle view of the geometry setup with the shielding wall included.

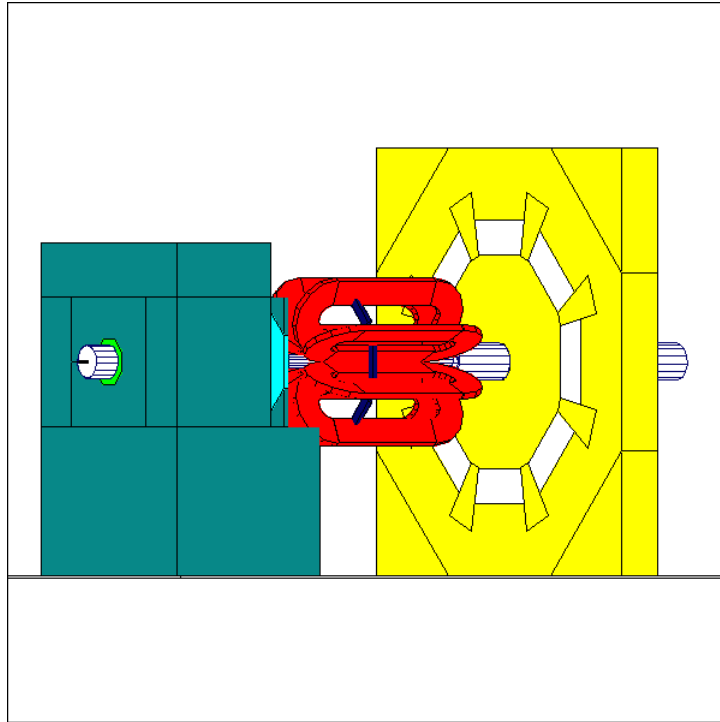


Figure 14: Side-angle view of the GEANT3 simulation geometry with the shielding wall.

References

- [1] J. Birchall. Update of systematic errors in Qweak. Collaboration meeting talk, 2008.
Qweak document: <http://qweak.jlab.org/doc-private/ShowDocument?docid=725>.